ACS APPLIED ENERGY MATERIALS

www.acsaem.org Article

Hybrid CuFe–CoFe Prussian Blue Catalysts on $BiVO_4$ for Enhanced Charge Separation and Injection for Photoelectrochemical Water Oxidation

Emre Usman,[#] Mahsa Barzgar Vishlaghi,[#] Sina Sadigh Akbari,[#] Ferdi Karadaş,[*] and Sarp Kaya[*]

Cite This: *ACS Appl. Energy Mater.* 2022, 5, 15434–15441 Read Online

ACCESS | Metrics & More | Article Recommendations | Supporting Information

ABSTRACT: The utilization of cocatalysts on the photoelectrode surface is a feasible strategy to achieve a high photocurrent density in the photoelectrochemical water oxidation process. The catalysts can enhance the activity by improving the reaction kinetics, retarding charge carrier recombination, or accumulating charge carriers. In this work, we have utilized a CuFe–CoFe Prussian blue (PB) catalyst layer on the $BiVO_4$ photoanode surface to enhance its water oxidation activity. The hybrid catalyst, in which the semiprecious cobalt ions are partially substituted with earth-abundant copper ions, exhibits 56% higher photocurrent density than the CoFe PB-modified $BiVO_4$. We show that photogenerated hole accumulation is present in the CuFe PB layer, which results in higher charge extraction from the $BiVO_4$ surface. The CoFe PB layer on top of the CuFe one facilitates the charge transfer due to its catalytic activity toward the oxygen evolution reaction (OER).

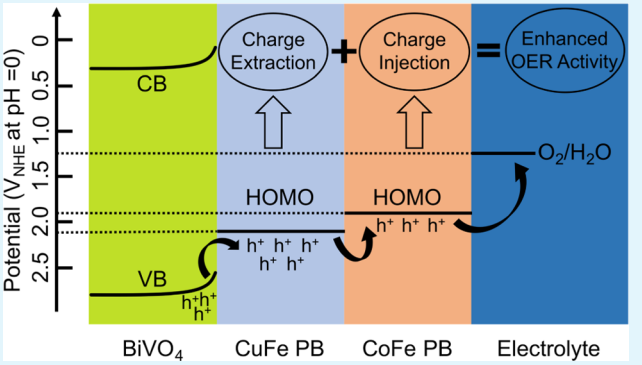

KEYWORDS: *photoelectrochemical conversion, water splitting, Prussian blue, $BiVO_4$, OER, charge extraction*

INTRODUCTION

Limited resources of fossil fuels as the main energy supply in the world and their unsustainability have raised a worldwide concern. Photoelectrochemical water splitting, which converts solar energy into chemical fuels, has been regarded as a promising method for sustainable energy production.[1−3] In semiconductor-based solar water splitting devices, photogenerated electrons in the cathode run the reduction reaction ending up in hydrogen production, while photogenerated holes in the anode drive the water oxidation reaction.[3] Such semiconductors have band edge positions straddling the water oxidation and water reduction electrochemical potentials. Since the water oxidation process is the rate-limiting process, limiting the overall hydrogen production rate due to the sluggish kinetics, a great deal of effort has been devoted to developing photoanode materials with faster water oxidation kinetics.[4] As a promising photoanode material for solar water splitting, $BiVO_4$ has attracted attention due to its proper band gap for sunlight absorption (2.4 eV). Moreover, it exhibits appropriate proper valence band edge position[5] compared to the electrochemical potential of the water oxidation reaction, providing enough driving force for the photogenerated holes to run the oxygen evolution reaction.[6,7] However, it suffers from slow charge transfer kinetics at the surface. A wide variety of catalysts including CoO_x, NiO, NiOOH, FeOOH, CoBi, and CoPi[8−12] have been used to overcome the poor catalytic activity of $BiVO_4$ by increasing the charge transfer kinetics at the solid–liquid interface. The relatively poor catalytic activity of $BiVO_4$ is also due to the charge recombination at the surface defects. It is shown that CoPi enhances the water oxidation kinetics at the $BiVO_4$ surface by blocking the surface defects that serve as charge recombination sites rather than promoting the hole transfer to the electrolyte.[12] Interestingly, some oxide materials that are not OER catalysts have been observed also to boost $BiVO_4$ performance. An ultrathin TiO_2 layer is shown to enhance the photocurrent of $BiVO_4$ due to suppression of electron trapping at surface states and enhancement of the electron photoconductivity.[13] Another type of catalyst, which has shown a strong water oxidation activity is metal-based Prussian blue (PB) analogues that are successfully implemented for $BiVO_4$ photoanodes.[14−16]

Cobalt-based PB analogues, CoM PBs (M = Co, Fe), have recently emerged as promising materials for the water oxidation reaction due to their high stabilities and activities as water oxidation catalysts.[17−20] The metal ions are connected through a cyanide group (CN^-) to construct a robust

Received: September 18, 2022
Accepted: November 15, 2022
Published: December 1, 2022

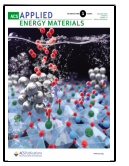

coordination polymer that is stable and active in a wide pH range, pH 1−13.[16] In a typical CoM PB structure, M sites, which are coordinated by six cyanide groups, are catalytically inactive. In contrast, cobalt sites are surrounded by a combination of nitrogen atoms of cyanide groups and water molecules, making them suitable catalytic centers for the water oxidation process. Coupling PB with an appropriate photosensitizer and/or a semiconductor to use them in the light-driven water oxidation process is the general approach due to the poor photocurrent efficiency of PBs.[18,21−24] In such a design, the valence band of the semiconductor should be located at lower energy than the highest occupied molecular orbital (HOMO) level of the PB for an efficient charge transfer. Goberna-Ferron and co-workers studied a catalyst screening of PB with various metals (Mn−Fe, Fe−Fe, Co−Fe, Ni−Fe, Cu−Fe, Mn−Co, Fe−Co, and Co−Co) for the photocatalytic water oxidation process in the presence of a ruthenium photosensitizer. Their study showed that PBs containing Mn^{2+} or Co^{2+} have catalytic activities for the OER[18] with slower kinetics for MnFe PB than CoFe PBs. They reported that the presence of Co in a PB-type structure serves as an efficient catalytic site for the OER, which is compatible with classical metal oxides. A CoFe PB layer on a semiconductor is also observed to improve the hole transfer at the surface via different mechanisms. Hegner and co-workers compared the photoelectrochemical activity of CoFe PB with other Co-based catalysts to reveal that a CoFe PB layer raises the photocurrent significantly due to a proper valence band alignment with $BiVO_4$[25] and an adequate interface between the catalyst and $BiVO_4$. Moss and co-workers showed that an irreversible charge transfer from CoFe PB to $BiVO_4$ occurs, resulting in a hole accumulation in the CoFe PB layer and retardation of charge recombination.[26] Similarly, Li et al. reported that CoFe PB acts as a hole storage layer on $BiVO_4$ photoanode and accelerates charge transfer through the interface.[27] Despite the growing number of efforts on improving the activity of $BiVO_4$ with Co-based PBs, the effect of a second metal ion on the activity of Co-based PB layers has not been investigated yet. Furthermore, partial substitution of semiprecious cobalt ions with relatively nontoxic, abundant, and low-cost 3d metal ions could pave the way for the development of low-cost PB-based photoanodes.

The insertion of a CuFe layer into a Co-based PB layer could be a novel approach to unify the strengths of Cu and Co, which exhibit remarkable charge transfer properties and high catalytic activities, respectively. Recently, Yamada et al. showed that the photocatalytic activity of CoFe PB can be enhanced by increasing the intrinsic defect sites with the formation of a CoFe/CuFe PB core−shell structure.[28] In this work, we prepared a series of PB-coated $BiVO_4$ photoelectrodes with different Cu:Co atomic ratios to elucidate the effect of Cu and Co sites on the performance of the photoanode. We showed that CuFe−CoFe PB layers on $BiVO_4$ enhance the photocurrent and IPCE more than CoFe PB despite the better catalytic activity of Co for the OER compared to Cu. A CuFe layer between $BiVO_4$ and CoFe has been shown to ease the charge transfer from $BiVO_4$ to CoFe and improve the charge separation, while the CoFe layer acts as an OER catalyst at the $BiVO_4$ surface. This study shows the importance of catalysts and replacing rare and toxic catalysts with earth-abundant and safe ones, which can be a motivation for optimum catalyst design.

EXPERIMENTAL METHODS

Materials. Vanadyl acetyl acetonate ($VO(acac)_2$, 98%), bismuth nitrate pentahydrate ($Bi(NO_3)_3{\cdot}5H_2O$, ≥99.99%), *p*-benzoquinone ($C_6H_4O_2$, ≥98%), ethanol (C_2H_5OH, ≥99.8%), DMSO (C_2H_6OS, ≥99.5%), sodium iodide (NaI, ≥99.5%), potassium hexacyanoferrate ($K_3[Fe(CN)_6]$, ≥99.5%), and nitric acid solution (HNO_3, 70% w/w) were purchased from Sigma-Aldrich. Cobalt nitrate hexahydrate ($Co(NO_3)_2{\cdot}6H_2O$, ≥99.9%) and copper nitrate trihydrate ($Cu(NO_3)_2{\cdot}3H_2O$, ≥99.9%) were obtained from Alfa Aesar. Sodium hydroxide (NaOH, 99%), dipotassium phosphate (K_2HPO_4, 98−101%), monopotassium phosphate (KH_2PO_4, 99.5−100.5%), and sodium sulfite (Na_2SO_3, ≥98.0%) were purchased from ISOLAB. FTO-coated glasses (fluorinated tin oxide, 6−9 $\Omega{\cdot}sq^{-1}$) were purchased from Ossila. Ultrapure water (18.2 MΩ·cm) from ELGA Purelab Flex was used to prepare the solutions. All of the chemicals were used without any other purification procedure.

$BiVO_4$ Photoanode Fabrication. The $BiVO_4$ photoanodes were prepared using the electrodeposition method, which was previously reported elsewhere.[9] First, the FTOs on glass substrates were cleaned by sonication in ethanol, acetone, and ultrapure water for 10 min each. To prepare the plating solution for electrochemical deposition, first, 1.49 g of NaI (0.4 M) was dissolved in 25 mL of ultrapure water. The pH of the solution was adjusted to 1.8 with diluted HNO_3 solution. Then, 485 mg of bismuth nitrate pentahydrate (0.04 M) was added to the solution and stirred for 30 min, until complete dissolution. Another solution was prepared by dissolving 249 mg of *p*-benzoquinone (0.23 M) in 10 mL of ethanol. Then, these solutions were mixed and stirred for additional 30 min. The electrodeposition was done using a VSP-300 potentiostat and a three-electrode configuration. A platinum wire was used as the counter electrode, an Ag/AgCl (sat'd KCl) electrode was utilized as the reference electrode, and the FTO substrate was used as the working electrode. The electrodeposition was done with −0.1 V bias vs the reference electrode for 2 min to obtain a BiOI film. After electrodeposition, the electrodes were cleaned with ultrapure water and dried in air at room temperature. Then, 530 mg of vanadyl acetyl acetonate (0.4 M) was dissolved in 5 mL of DMSO, and 2 μL of this solution was dropped on BiOI films with a 1 cm^2 geometric area. After 5 min of waiting for $VO(acac)_2$ solution to penetrate into the porous BiOI film, the excess solution was removed by touching the edge of the substrate with a filter paper. The samples were annealed in a muffle furnace in air at 450 °C for 2 h with a ramping rate of 2 $°C{\cdot}min^{-1}$. Then, the photoanodes were soaked in 1 M sodium hydroxide solution for 30 min to remove the excess V_2O_5 impurity at the surface. As a final step, the photoanodes were further annealed at 200 °C with flowing O_2 gas in a tubular furnace for 2 h.[29]

Prussian Blue Coating. The deposition of PB on the $BiVO_4$ electrodes was performed according to a two-stage procedure. First, the electrodes were dipped in a $K_3[Fe(CN)_6]$ solution (0.02 M in H_2O) for 10 min with gentle stirring to bind $Fe(CN)_6^{3-}$ on the surface of the $BiVO_4$ layer. After thoroughly rinsing the electrodes with deionized water, they were dipped in the $M^{2+}(NO_3)_2$ solution (0.04 M in H_2O; M^{2+}: Co^{2+} or Cu^{2+}) for 10 min under stirring to form the PB structure. The sequence was repeated six times for CoFe PB- and CuFe PB-modified electrodes. CoCuFe/$BiVO_4$ electrodes were coated first with five layers of CuFe PB and then one layer of CoFe PB.

PEC Measurements. PEC tests were carried out using a VSP-300 Biologic potentiostat using a three-electrode configuration. A Pt wire was used as the counter electrode, and Ag/AgCl (sat'd KCl) was used as the reference electrode, similar to the electrodeposition setup. As a solar simulator, an Oriel LCS-100 with a 100 W Xe lamp and an AM1.5G filter was used. The intensity of light on the photoanodes was calibrated to 100 $mW{\cdot}cm^{-2}$ with a thermal power sensor. The potential values were converted to vs reversible hydrogen electrode (RHE) using the Nernst equation, which is given below

$$V_{RHE} = V_{Ag/AgCl} + 0.059 \times pH + V^{\circ}_{Ag/AgCl} \quad (1)$$

https://doi.org/10.1021/acsaem.2c03038
ACS Appl. Energy Mater. 2022, 5, 15434−15441

where V_{RHE} is the potential with respect to the RHE, $V_{Ag/AgCl}$ is the potential with respect to the reference electrode, pH is the pH of the electrolyte solution, and $V^{\circ}_{Ag/AgCl}$ is the standard potential of the reference electrode, which is 0.197 V_{NHE}. Potassium phosphate buffer (KPi) (0.1 M) at pH = 7, with or without 0.5 M Na_2SO_3, was used as the electrolyte solution. The linear sweep voltammetry (LSV) measurements were performed using 50 $mV{\cdot}s^{-1}$ potential scan rate. For the transient photocurrent (TPC) measurements, a white light-emitting diode (LED) light was used with a pulse duration of 50.0 ms. The distance between the white LED source and the sample was kept at 10 cm, where the intensity of light was measured to be 15.0 $mW{\cdot}cm^{-2}$. The photocurrent responses were measured every 400.0 μs. The electrochemical impedance spectroscopy (EIS) measurements were done potentiostatically at different potentials with 10 mV signal amplitude and frequencies between 10^5 and 10^{-1} Hz. Incident photon-to-current efficiency (IPCE) measurements were done using a Newport monochromator with a 300 W Xenon lamp. IPCE values were calculated with the equation below

$$\mathrm{IPCE} = \frac{[j\ (\mathrm{mA{\cdot}cm^{-2}}) \times 1240\ (\mathrm{V{\cdot}nm})]}{[P_\lambda\ (\mathrm{mW{\cdot}cm^{-2}}) \times \lambda\ (\mathrm{nm})]} \quad (2)$$

where j is the photocurrent density, λ is the wavelength of the incident light, and P_λ is the power of the incident light at wavelength λ.

Structural Characterizations. X-ray photoelectron spectroscopy (XPS) measurements were performed using a Thermo K-alpha laboratory XPS system with a monochromatized Al Kα X-ray source. Raman spectra were obtained using a Renishaw INVIA spectrometer with a 532 nm laser as an excitation source.

RESULTS AND DISCUSSION

The bare $BiVO_4$ photoanodes were modified with three different PB catalysts. The photoanodes, which were dip-coated with six layers of CoFe PB, are denoted by CoFe/$BiVO_4$. CoCuFe/$BiVO_4$ photoanodes were modified with five layers of CuFe and then one layer of CoFe. The CuFe/$BiVO_4$ photoanodes were dip-coated with six layers of CuFe PB (Figure S1).

The $BiVO_4$ photoanodes modified at the surface with PBs were characterized by XPS, as shown in Figure 1. The Co $2p_{3/2}$ peak located at 781 eV for CoFe/$BiVO_4$ and CoCuFe/$BiVO_4$ (Figure 1a) suggests that Co^{2+} sites are present on the surface of both electrodes.[30] The binding energy difference between Co $2p_{3/2}$ and $2p_{1/2}$ can be informative regarding the oxidation state of Co ions. A difference of 15 and 16 eV is indicative of 3+ and 2+ states, respectively.[31,32] The binding energy difference of 15.6 eV in the PB-modified $BiVO_4$ indicates the presence of a mixture of 2+ and 3+ oxidation states, which is typically observed for CoFe PBs.[18,33,34] Cu $2p_{3/2}$ has two distinct features; a peak at 935 eV with a broad satellite peak at around 943 eV (Figure 1b) is characteristic of a Cu^{2+} state, while the peak at 933 eV may be related to metallic Cu or Cu^{+}.[35] To distinguish these species from each other, we look at the Cu LMM Auger spectra (Figure 1c), revealing a broad peak at 916 eV that can be attributed to the Cu^{+} state.[36] Fe 2p spectra in Figure 1d show peaks for Fe $2p_{3/2}$ at 708.3 eV, suggesting that the majority of Fe^{3+} sites is reduced to Fe^{2+} during the fabrication of electrodes either by oxidizing Co sites, by transferring holes to $BiVO_4$, or a combination of both.[37] Bi 4f, V 2p, N 1s, and O 1s spectra are shown in Figure S2. Bi 4f and V 2p XPS spectra suggest Bi^{3+} and V^{5+} valence states,[38] respectively, which is consistent with the previous reports.[39,40] N 1s spectra show a peak at 397.7 eV attributed to N in cyanide groups.[41] In the O 1s spectra, there are two distinct peaks located at 529.8 and 531.0 eV that can be attributed to lattice oxygen in the bulk of the $BiVO_4$ and the surface hydroxyl groups, respectively.[42,43] The Raman spectra given in Figure S3 show a peak at 2110 cm^{-1} for all three photoanodes, which is associated with the vibration of the cyanide group coordinated to Fe^{2+}, consistent with the XPS results.[44,45]

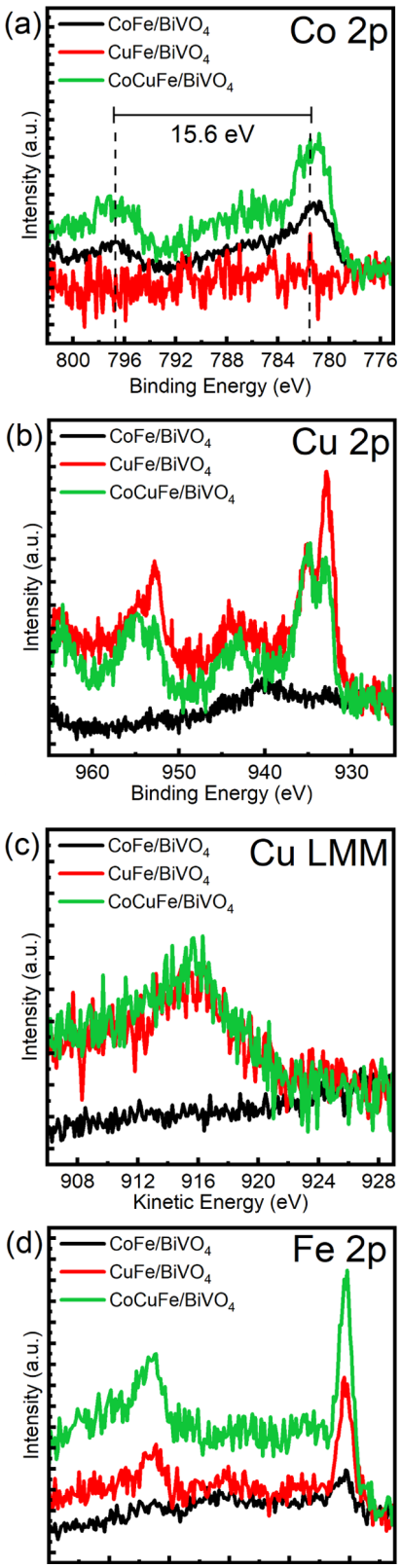

Figure 1. XPS measurements of CoFe-, CuFe-, and CoCuFe-modified $BiVO_4$ photoanodes. (a) Co 2p, (b) Cu 2p, (c) Cu LMM, and (d) Fe 2p XPS spectra.

https://doi.org/10.1021/acsaem.2c03038
ACS Appl. Energy Mater. 2022, 5, 15434−15441

To assess the water oxidation activities of these photoelectrodes, we have carried out linear sweep voltammetry (LSV), incident photon-to-current efficiency (IPCE), and electrochemical impedance spectroscopy (EIS) measurements in the absence of a sacrificial agent. Figure 2a shows that

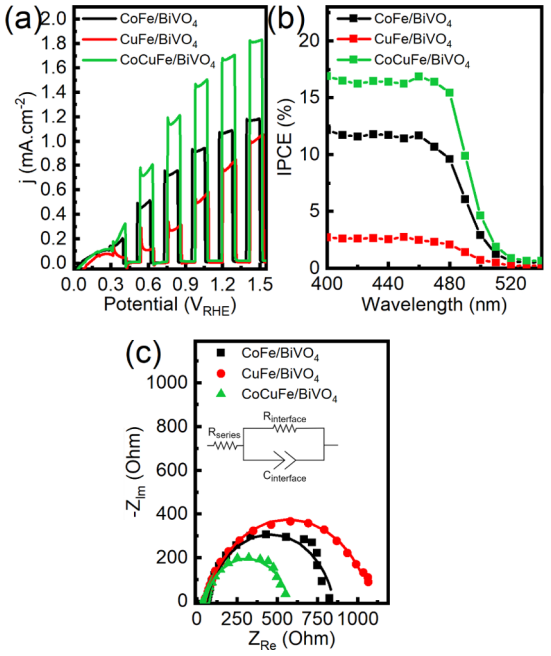

Figure 2. For CoFe, CuFe, and CoCuFe PB-modified $BiVO_4$ photoanodes, (a) LSV with chopped illumination, (b) IPCE at 1.23 V_{RHE}, and (c) EIS measurements at 0.8 V_{RHE} under front illumination in 0.1 M KPi buffer solution (pH = 7).

$CoFe/BiVO_4$ exhibits a photocurrent density of 1.07 $mA{\cdot}cm^{-2}$ at 1.23 V_{RHE}. $CoCuFe/BiVO_4$ on the other hand shows an enhanced photocurrent density of 1.67 $mA{\cdot}cm^{-2}$, demonstrating 56% higher activity than $CoFe/BiVO_4$. $CuFe/BiVO_4$ shows the lowest photocurrent among these photoanodes with a photocurrent density of 0.77 $mA{\cdot}cm^{-2}$ at 1.23 V_{RHE}. The IPCE results, which are given in Figure 2b, also confirm the superior activity of CoCuFe-modified photoanode as it results in a 17% efficiency, whereas CoFe has a 12% and CuFe has a 3% efficiency at 400 nm. EIS measurements were also carried out, and the Nyquist plots were fitted using the Randles model with a constant phase element. The equivalent circuit is given as an inset in Figure 2c, which consists of R_s (the Ohmic resistance in the electrochemical cell because of the electrolyte, wires, and electrical contacts), R_{ct} (the charge transfer resistance across the interface), and CPE (the capacitance at the photoanode/electrolyte interface).[46] The Nyquist plots show that the charge transfer resistance for the $CoFe/BiVO_4$ is 790 Ω, whereas $CoCuFe/BiVO_4$ demonstrates a lower resistance of 520 Ω. On the other hand, CuFe modification increases the resistance to 1030 Ω. These results suggest that the presence of CoFe on the surface is crucial for the enhancement of $BiVO_4$ water oxidation activity. However, this activity can be further enhanced by adding an interfacial layer of CuFe between $BiVO_4$ and the CoFe PB. The lowest activity is observed for $CuFe/BiVO_4$, confirming that the surface Co ions are critical for the high water oxidation performance.

To decouple the catalytic activity and the charge separation efficiency of the PB-modified photoanodes, we measured LSVs in the presence of 0.5 M Na_2SO_3 as a hole scavenger, which is given in Figure S4. The charge injection and charge separation efficiency values are given in Figure 3a,b, respectively. The

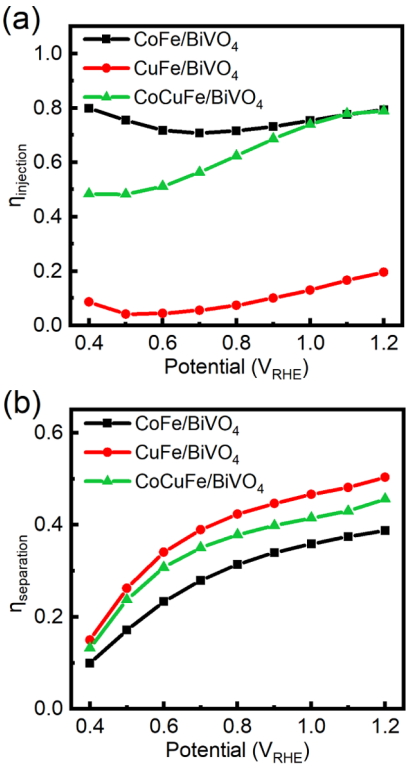

Figure 3. (a) Charge injection and (b) separation efficiency values for PB-modified $BiVO_4$ photoanodes.

details of the calculation are given in the SI. $CoFe/BiVO_4$ shows the highest charge injection efficiency among all photoanodes. Such behavior is expected since the enhancement of the catalytic activity of Co-based catalysts,[8,47−49] and more specifically, CoFe PB[14,25,26] on $BiVO_4$ has been well studied. $CoCuFe/BiVO_4$ on the other hand shows lower charge injection efficiency than $CoFe/BiVO_4$ at potentials between 0.4 and 0.9 V_{RHE} and very similar injection efficiency in the 1.0−1.2 V_{RHE} range. $CuFe/BiVO_4$ injection efficiency is observed only in the 0−0.2 potential range, suggesting very low catalytic turnover. Interestingly, these photoanodes demonstrate the highest charge separation efficiency, as shown in Figure 3b. The charge separation efficiency shows the following order: $CuFe/BiVO_4$ > $CoCuFe/BiVO_4$ > $CoFe/BiVO_4$. These findings suggest that the presence of CuFe PB at the $BiVO_4$ surface can enhance its charge separation properties without improving the catalytic activity. The role of CoFe PB, on the other hand, is attributed to its catalytic activity toward OER, resulting in an enhanced charge injection efficiency.

As shown in our earlier works on $BiVO_4$ photoanodes,[13,50] TPC measurements performed with 50.0 ms white LED short pulses can be used to acquire information about surface charge carrier dynamics in the millisecond time regime. We have carried out these measurements in the potential regime of 0.4−1.0 V_{RHE} with 0.1 V increments. Figure 4a−c shows the TPC results for $CoFe/BiVO_4$, $CuFe/BiVO_4$, and $CoCuFe/BiVO_4$, respectively. When we turn the light on at t = 0.0 ms, we observe an anodic increase in photocurrent in the first few milliseconds, resulting from charge generation and hole

https://doi.org/10.1021/acsaem.2c03038
ACS Appl. Energy Mater. 2022, 5, 15434−15441

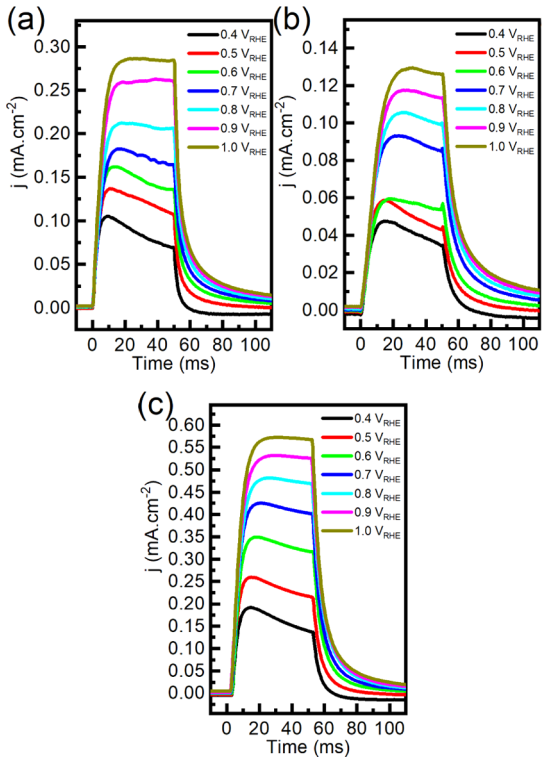

Figure 4. TPC measurements done using 50.0 ms white light LED short pulses in 0.1 M KPi buffer solution for (a) CoFe/$BiVO_4$, (b) CuFe/$BiVO_4$, and (c) CoCuFe/$BiVO_4$.

migration toward the surface. For each photoanode, the anodic increase in photocurrent increases with applied potential due to increasing band bending with the anodic polarization. Then, the photocurrent decays to a steady-state value due to the hole accumulation at the interface and catalytic limitations toward OER. The steady-state photocurrent density of the photoanodes follows the trend CoCuFe > CoFe > CuFe, which is consistent with the LSV, EIS, and IPCE results. For CoFe/$BiVO_4$ photoanode, the photocurrent decays when the light is turned on for applied potentials of 0.4−0.8 V_{RHE}. However, we do not observe a significant decay in photocurrent at potentials between 0.8 and 1.0 V_{RHE}, which suggests low hole accumulation and decent catalytic activity at these potentials. For CuFe/$BiVO_4$, we observe a decay in photocurrent at all potentials with a lower photocurrent density, suggesting low catalytic activity. For CoCuFe/$BiVO_4$, we observe a decay at potentials between 0.4 and 0.8 V_{RHE} and no decay at 0.8−1.0 V_{RHE} similar to CoFe/$BiVO_4$. When the light is turned off at t = 50.0 ms, holes accumulated on the surface recombine with the electrons, and the photocurrent decays to zero. It is also noteworthy that we observe a small anodic peak when we turn the light off for the CuFe/$BiVO_4$ photoanode. We previously attributed this peak to the photogenerated electron detrapping from the $BiVO_4$ surface due to the V^{5+}/V^{4+} surface state, where we showed that such phenomena could limit the water oxidation activity.[13] However, the extent of the detrapping phenomena is not significant; therefore, we leave it out of this discussion. The rate of the photocurrent decay after the light is turned off can give information about the existing charge carrier trapping or localization on the surface.[51] The localized holes in midgap states may recombine slower than the holes in the valence band. We have fitted the decay kinetics of the TPC measurements using two exponential decay functions and calculated the time constants, which are given in Figure S5. The average time constants for the CuFe/$BiVO_4$ photoanodes are higher at all potentials, suggesting that the decay is slower. On the other hand, CoFe and CoCuFe time constants are lower and comparable to each other. The slower decay can be an indication of hole trapping in the CuFe-modified photoanodes. The Cu 2p XPS and LMM Auger spectra given in Figure 1b,c show that Cu^+ species are present in the photoanode surfaces, as well as Cu^{2+}, suggesting that hole localization is viable in these sites. For CoFe- and CoCuFe-modified photoanodes, the hole trapping is not as significant as CuFe/$BiVO_4$. Therefore, we attribute the role of the CuFe PB layer as a hole extraction layer from the $BiVO_4$ surface, which enhances the charge separation properties of $BiVO_4$. The role of the CoFe PB layer is mostly catalytic. In the CoFe photoanodes, the photogenerated holes from the $BiVO_4$ surface are transferred to the CoFe layer to be utilized for the catalytic water oxidation process on the Co sites. For the CuFe-modified electrode, the photogenerated holes may transfer to the CuFe layer; however, due to sluggish OER kinetics of the Cu ions, the holes cannot be transfered to the electrolyte effectively, resulting in poor photocurrent. For the CoCuFe/$BiVO_4$ photoanode, we propose that two layers of PB can have a synergistic effect, in which the photogenerated holes near the surface region of $BiVO_4$ can get trapped in the CuFe layer, to be transferred efficiently to the CoFe PB layer for the OER process.

We have carried out EIS measurements in the potential region of 0.4−1.0 V_{RHE} to gain insights into the interfacial charge transfer resistance and the capacitance of the PB-modified photoanodes. Figure 5a,b shows the charge transfer resistance and the capacitance values at the interface as a function of the applied potential, respectively. The Nyquist

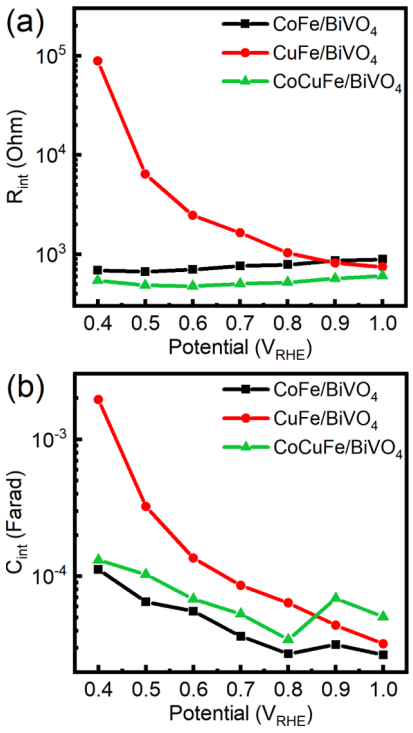

Figure 5. Potential-dependent EIS measurements and fitting parameters of (a) R_{ct}, and (b) C_{int} performed under front illumination in 0.1 M KPi buffer solution.

https://doi.org/10.1021/acsaem.2c03038
ACS Appl. Energy Mater. 2022, 5, 15434−15441

plots of the EIS measurements and the fittings are given in Figure S6. The charge transfer resistance for the CoCuFe/$BiVO_4$ photoanode is the lowest, whereas CuFe/$BiVO_4$ shows significantly higher resistance. Such a behavior is expected as the Co ions can transfer holes more rapidly due to their catalytic activities, resulting in lower resistance for CoFe/$BiVO_4$ than CuFe/$BiVO_4$. CoCuFe/$BiVO_4$ has even lower R_{ct}, indicating superior OER activity. Capacitance measurements given in Figure 5b show higher C_{int} for CuFe/$BiVO_4$ photoanodes at all potentials, whereas CoFe/$BiVO_4$ photoanodes have the lowest capacitance. The capacitive behavior for a photoelectrode can result from the surface states, electrical double layer, and the space−charge capacitance.[52] C_{DL} measurements given in Figure S7 do not vary significantly between the photoanodes. The Mott−Schottky analysis in Figure S8 also does not yield a significantly different slope between the photoanodes, suggesting that the N_d values and thus the potential drop across the space−charge region are similar. The C_{int} under illumination can be associated with the accumulation of the positively charged species, namely, photogenerated holes, at the interface.[53] We propose that the C_{int} is larger for the CuFe-modified photoanode because of the photogenerated hole accumulation at the CuFe layer, resulting from available Cu sites for hole localization, consistent with the previous TPC and charge separation efficiency results. CoFe/$BiVO_4$ shows the lowest C_{int}, as the holes are effectively utilized for water oxidation and no significant accumulation occurs. CoCuFe/$BiVO_4$ on the other hand has both features, as the holes are extracted and accumulated in the CuFe PB layer and then transferred to the CoFe PB layer and utilized effectively for OER.

LSV measurements were carried out for CuFe/$BiVO_4$ and CoFe/$BiVO_4$ in the absence of illumination, which are given in Figure S9. The oxidation onset potentials can be used to determine the HOMO levels for the PB catalysts.[18] For CuFe and CoFe PB, HOMO levels can be estimated as 2.1 and 1.9 V_{RHE}, respectively. Thus, the relative band positions of $BiVO_4$, CuFe PB, and CoFe PB can be demonstrated as given in Figure 6. The relative positions of the valence band edge of

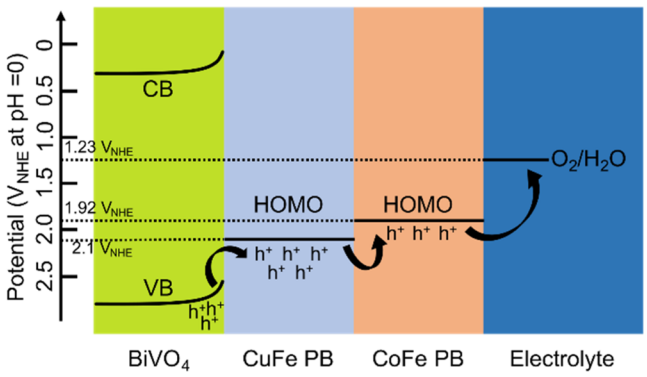

Figure 6. Schematic representation of the CoCuFe/$BiVO_4$ band diagram and the charge transfer pathway.

$BiVO_4$ and the HOMO levels of CuFe and CoFe PB show that the hole transfer toward the surface in such a configuration is feasible.

CONCLUSIONS

We have modified the $BiVO_4$ surface with a novel CoCuFe hybrid PB catalyst layer to enhance the charge injection and separation properties of $BiVO_4$. The CoCuFe PB modification yields a photocurrent density of 1.67 mA·cm^{-2}, showing 56% higher activity than that of the CoFe-coated photoanode. We corroborated the performance enhancement with the decrease of charge transfer resistance and increase of the IPCE. The CuFe PB-modified photoanode shows a slow photocurrent decay in the TPC measurements, higher capacitance under illumination, and enhanced charge separation. We attribute the enhancement with the CoCuFe PB modification to the synergistic effect of CuFe and CoFe PB catalyst layers. The CuFe PB layer can extract photogenerated holes from the $BiVO_4$ surface, and the CoFe layer facilitates the reaction kinetics of the OER, resulting in an enhanced photocurrent. Adding a CuFe layer between the $BiVO_4$ surface and the catalytic CoFe layer not only enhances the performance but also decreases the cost of the photoanode. In conclusion, we show that adding an interfacial layer could be a feasible strategy to enhance the activity of cocatalyst-modified $BiVO_4$ photoanodes further and decrease their cost.

ASSOCIATED CONTENT

Supporting Information

The Supporting Information is available free of charge at https://pubs.acs.org/doi/10.1021/acsaem.2c03038.

Schematic representations of the photoanodes, XPS and Raman spectra, performance comparison with the literature, LSV in scavenger solution, TPC average decay constants, Nyquist plots, C_{DL} measurements, Mott−Schottky analysis, stability measurements, and CV with the absence of illumination (PDF)

AUTHOR INFORMATION

Corresponding Authors

Ferdi Karadaş − *UNAM-National Nanotechnology Research Center, Institute of Materials Science and Nanotechnology, Bilkent University, 06800 Ankara, Turkey; Department of Chemistry, Bilkent University, 06800 Ankara, Turkey*; Email: karadas@fen.bilkent.edu.tr

Sarp Kaya − *Materials Science and Engineering, Koç University, 34450 Istanbul, Turkey; Koç University Tüpraş Energy Center (KUTEM), 34450 Istanbul, Turkey; Department of Chemistry, Koç University, 34450 Istanbul, Turkey*; orcid.org/0000-0002-2591-5843; Email: sarpkaya@ku.edu.tr

Authors

Emre Usman − *Materials Science and Engineering, Koç University, 34450 Istanbul, Turkey; Koç University Tüpraş Energy Center (KUTEM), 34450 Istanbul, Turkey;* Present Address: Department of Chemistry, University of Wisconsin-Madison, Madison, Wisconsin 53706, United States

Mahsa Barzgar Vishlaghi − *Materials Science and Engineering, Koç University, 34450 Istanbul, Turkey; Koç University Tüpraş Energy Center (KUTEM), 34450 Istanbul, Turkey;* Present Address: Helmholtz-Zentrum Berlin für Materialien und Energie, 14109 Berlin, Germany.

https://doi.org/10.1021/acsaem.2c03038
ACS Appl. Energy Mater. 2022, 5, 15434−15441

Sina Sadigh Akbari − *UNAM-National Nanotechnology Research Center, Institute of Materials Science and Nanotechnology, Bilkent University, 06800 Ankara, Turkey; Department of Chemistry, Bilkent University, 06800 Ankara, Turkey*

Complete contact information is available at: https://pubs.acs.org/10.1021/acsaem.2c03038

Author Contributions

#E.U., M.B.V., and S.S.A. have contributed to this study equally.

Notes

The authors declare no competing financial interest.

■ ACKNOWLEDGMENTS

The authors would like to thank The Scientific and Technical Research Council of Turkey (TUBITAK) for support (Grant Number: 221Z070). The authors thank KUYTAM for the characterization measurements. The authors thank Elif Öykü Alagöz for her support.

■ REFERENCES

(1) Fujishima, A.; Honda, K. Electrochemical Photolysis of Water at a Semiconductor Electrode. *Nature* **1972**, *238*, 37−38.
(2) Tryk, D. A.; Fujishima, A.; Honda, K. Recent Topics in Photoelectrochemistry: Achievements and Future Prospects. *Electrochim. Acta* **2000**, *45*, 2363−2376.
(3) Photoelectrochemical Hydrogen Production: *Electronic Materials: Science & Technology*; Krol, R.; van de Grätzel, M., Eds.; Springer: New York, 2012; pp 3−13.
(4) Kim, J. H.; Lee, J. S. Elaborately Modified BiVO $_4$ Photoanodes for Solar Water Splitting. *Adv. Mater.* **2019**, *31*, No. 1806938.
(5) Sivula, K.; van de Krol, R. Semiconducting Materials for Photoelectrochemical Energy Conversion. *Nat. Rev. Mater.* **2016**, *1*, No. 15010.
(6) Huang, Z.-F.; Pan, L.; Zou, J.-J.; Zhang, X.; Wang, L. Nanostructured Bismuth Vanadate-Based Materials for Solar-Energy-Driven Water Oxidation: A Review on Recent Progress. *Nanoscale* **2014**, *6*, 14044−14063.
(7) Park, Y.; McDonald, K. J.; Choi, K.-S. Progress in Bismuth Vanadate Photoanodes for Use in Solar Water Oxidation. *Chem. Soc. Rev.* **2013**, *42*, 2321−2337.
(8) Barzgar Vishlaghi, M.; Kahraman, A.; Apaydin, S.; Usman, E.; Aksoy, D.; Balkan, T.; Munir, S.; Harfouche, M.; Ogasawara, H.; Kaya, S. The Significance of the Local Structure of Cobalt-Based Catalysts on the Photoelectrochemical Water Oxidation Activity of BiVO4. *Electrochim. Acta* **2021**, *366*, No. 137467.
(9) Kim, T. W.; Choi, K.-S. Nanoporous $BiVO_4$ Photoanodes with Dual-Layer Oxygen Evolution Catalysts for Solar Water Splitting. *Science* **2014**, *343*, 990−994.
(10) Lu, Y.; Yang, Y.; Fan, X.; Li, Y.; Zhou, D.; Cai, B.; Wang, L.; Fan, K.; Zhang, K. Boosting Charge Transport in BiVO4 Photoanode for Solar Water Oxidation. *Adv. Mater.* **2022**, *34*, No. 2108178.
(11) Jin, B.; Cho, Y.; Park, C.; Jeong, J.; Kim, S.; Jin, J.; Kim, W.; Wang, L.; Lu, S.; Zhang, S.; Oh, S. H.; Zhang, K.; Park, J. H. A Two-Photon Tandem Black Phosphorus Quantum Dot-Sensitized BiVO4 Photoanode for Solar Water Splitting. *Energy Environ. Sci.* **2022**, *15*, 672−679.
(12) Zachäus, C.; Abdi, F. F.; Peter, L. M.; van de Krol, R. Photocurrent of BiVO $_4$ Is Limited by Surface Recombination, Not Surface Catalysis. *Chem. Sci.* **2017**, *8*, 3712−3719.
(13) Usman, E.; Barzgar Vishlaghi, M.; Kahraman, A.; Solati, N.; Kaya, S. Modifying the Electron-Trapping Process at the BiVO4 Surface States via the TiO2 Overlayer for Enhanced Water Oxidation. *ACS Appl. Mater. Interfaces* **2021**, *13*, 60602−60611.
(14) Ghobadi, T. G. U.; Ghobadi, A.; Soydan, M. C.; Vishlaghi, M. B.; Kaya, S.; Karadas, F.; Ozbay, E. Strong Light−Matter Interactions in Au Plasmonic Nanoantennas Coupled with Prussian Blue Catalyst on BiVO $_4$ for Photoelectrochemical Water Splitting. *ChemSusChem* **2020**, *13*, 2577−2588.
(15) Ulusoy Ghobadi, T. G.; Akhuseyin Yildiz, E.; Buyuktemiz, M.; Sadigh Akbari, S.; Topkaya, D.; İsci, Ü.; Dede, Y.; Yaglioglu, H. G.; Karadas, F. A Noble-Metal-Free Heterogeneous Photosensitizer-Relay Catalyst Triad That Catalyzes Water Oxidation under Visible Light. *Angew. Chem., Int. Ed.* **2018**, *57*, 17173−17177.
(16) Han, L.; Tang, P.; Reyes-Carmona, Á.; Rodríguez-García, B.; Torréns, M.; Morante, J. R.; Arbiol, J.; Galan-Mascaros, J. R. Enhanced Activity and Acid PH Stability of Prussian Blue-Type Oxygen Evolution Electrocatalysts Processed by Chemical Etching. *J. Am. Chem. Soc.* **2016**, *138*, 16037−16045.
(17) Turhan, E. A.; Nune, S. V. K.; Ülker, E.; Şahin, U.; Dede, Y.; Karadas, F. Water Oxidation Electrocatalysis with a Cobalt-Borate-Based Hybrid System under Neutral Conditions. *Chem. - Eur. J.* **2018**, *24*, 10372−10382.
(18) Akbari, S. S.; Unal, U.; Karadas, F. Photocatalytic Water Oxidation with a CoFe Prussian Blue Analogue−Layered Niobate Hybrid Material. *ACS Appl. Energy Mater.* **2021**, *4*, 12383−12390.
(19) Akbari, S. S.; Karadas, F. Precious Metal-Free Photocatalytic Water Oxidation by a Layered Double Hydroxide-Prussian Blue Analogue Hybrid Assembly. *ChemSusChem* **2021**, *14*, 679−685.
(20) Pintado, S.; Goberna-Ferrón, S.; Escudero-Adán, E. C.; Galán-Mascarós, J. R. Fast and Persistent Electrocatalytic Water Oxidation by Co−Fe Prussian Blue Coordination Polymers. *J. Am. Chem. Soc.* **2013**, *135*, 13270−13273.
(21) Goberna-Ferrón, S.; Hernández, W. Y.; Rodríguez-García, B.; Galán-Mascarós, J. R. Light-Driven Water Oxidation with Metal Hexacyanometallate Heterogeneous Catalysts. *ACS Catal.* **2014**, *4*, 1637−1641.
(22) Chalil Oglou, R.; Ulusoy Ghobadi, T. G.; Ozbay, E.; Karadas, F. "Plug and Play" Photosensitizer−Catalyst Dyads for Water Oxidation. *ACS Appl. Mater. Interfaces* **2022**, *14*, 21131−21140.
(23) Gundogdu, G.; Ghobadi, T. G. U.; Akbari, S. S.; Ozbay, E.; Karadas, F. Photocatalytic Water Oxidation with a Prussian Blue Modified Brown TiO2. *Chem. Commun.* **2021**, *57*, 508−511.
(24) Ulusoy Ghobadi, T. G.; Ghobadi, A.; Buyuktemiz, M.; Yildiz, E. A.; Berna Yildiz, D.; Yaglioglu, H. G.; Dede, Y.; Ozbay, E.; Karadas, F. A Robust, Precious-Metal-Free Dye-Sensitized Photoanode for Water Oxidation: A Nanosecond-Long Excited-State Lifetime through a Prussian Blue Analogue. *Angew. Chem., Int. Ed.* **2020**, *59*, 4082−4090.
(25) Hegner, F. S.; Herraiz-Cardona, I.; Cardenas-Morcoso, D.; López, N.; Galán-Mascarós, J.-R.; Gimenez, S. Cobalt Hexacyanoferrate on BiVO4 Photoanodes for Robust Water Splitting. *ACS Appl. Mater. Interfaces* **2017**, *9*, 37671−37681.
(26) Moss, B.; Hegner, F. S.; Corby, S.; Selim, S.; Francàs, L.; López, N.; Giménez, S.; Galán-Mascarós, J.-R.; Durrant, J. R. Unraveling Charge Transfer in CoFe Prussian Blue Modified BiVO4 Photoanodes. *ACS Energy Lett.* **2019**, *4*, 337−342.
(27) Li, J.; Chu, Y.; Zhang, C.; Zhang, X.; Wu, C.; Xiong, X.; Zhou, L.; Wu, C.; Han, D. CoFe Prussian Blue Decorated BiVO4 as Novel Photoanode for Continuous Photocathodic Protection of 304 Stainless Steel. *J. Alloys Compd.* **2021**, *887*, No. 161279.
(28) Tabe, H.; Kitase, A.; Yamada, Y. Utilization of Core-Shell Nanoparticles to Evaluate Subsurface Contribution to Water Oxidation Catalysis of [CoII(H2O)2]1.5[CoIII(CN)6] Nanoparticles. *Appl. Catal., B* **2020**, *262*, No. 118101.
(29) Barzgar Vishlaghi, M.; Kahraman, A.; Kaya, S. Increasing Charge Separation Property and Water Oxidation Activity of BiVO $_4$ Photoanodes via a Postsynthetic Treatment. *J. Phys. Chem. C* **2020**, *124*, 1337−1345.
(30) Yang, J.; Liu, H.; Martens, W. N.; Frost, R. L. Synthesis and Characterization of Cobalt Hydroxide, Cobalt Oxyhydroxide, and Cobalt Oxide Nanodiscs. *J. Phys. Chem. C* **2010**, *114*, 111−119.

(31) Atzei, D.; Rossi, A.; Sadun, C. Synthesis and Characterization of a Cobalt(III) Complex with 1-(d-3-Mercapto-2-Methylpropionyl)-l-Proline. *Spectrochim. Acta, Part A* **2000**, *56*, 1875−1886.
(32) Briggs, D.; Gibson, V. A. Direct Observation of Multiplet Splitting in 2P Photoelectron Peaks of Cobalt Complexes. *Chem. Phys. Lett.* **1974**, *25*, 493−496.
(33) Lezna, R. O.; Romagnoli, R.; de Tacconi, N. R.; Rajeshwar, K. Cobalt Hexacyanoferrate: Compound Stoichiometry, Infrared Spectroelectrochemistry, and Photoinduced Electron Transfer. *J. Phys. Chem. B* **2002**, *106*, 3612−3621.
(34) Berrettoni, M.; Ciabocco, M.; Fantauzzi, M.; Giorgetti, M.; Rossi, A.; Caponetti, E. Physicochemical Characterization of Metal Hexacyanometallate−TiO2 Composite Materials. *RSC Adv.* **2015**, *5*, 35435−35447.
(35) Ghijsen, J.; Tjeng, L. H.; van Elp, J.; Eskes, H.; Westerink, J.; Sawatzky, G. A.; Czyzyk, M. T. Electronic Structure of Cu 2 O and CuO. *Phys. Rev. B* **1988**, *38*, 11322−11330.
(36) Poulston, S.; Parlett, P. M.; Stone, P.; Bowker, M. Surface Oxidation and Reduction of CuO and Cu2O Studied Using XPS and XAES. *Surf. Interface Anal.* **1996**, *24*, 811−820.
(37) Grosvenor, A. P.; Kobe, B. A.; Biesinger, M. C.; McIntyre, N. S. Investigation of Multiplet Splitting of Fe 2p XPS Spectra and Bonding in Iron Compounds. *Surf. Interface Anal.* **2004**, *36*, 1564−1574.
(38) Chen, L.; Alarcón-Lladó, E.; Hettick, M.; Sharp, I. D.; Lin, Y.; Javey, A.; Ager, J. W. Reactive Sputtering of Bismuth Vanadate Photoanodes for Solar Water Splitting. *J. Phys. Chem. C* **2013**, *117*, 21635−21642.
(39) Lu, X.; Ye, K.; Zhang, S.; Zhang, J.; Yang, J.; Huang, Y.; Ji, H. Amorphous Type FeOOH Modified Defective BiVO4 Photoanodes for Photoelectrochemical Water Oxidation. *Chem. Eng. J.* **2022**, *428*, No. 131027.
(40) Qin, D.-D.; Wang, T.; Song, Y.-M.; Tao, C.-L. Reduced Monoclinic BiVO4 for Improved Photoelectrochemical Oxidation of Water under Visible Light. *Dalton Trans.* **2014**, *43*, 7691.
(41) Wang, J.-G.; Zhang, Z.; Liu, X.; Wei, B. Facile Synthesis of Cobalt Hexacyanoferrate/Graphene Nanocomposites for High-Performance Supercapacitor. *Electrochim. Acta* **2017**, *235*, 114−121.
(42) Li, J.; Guo, L.; Lei, N.; Song, Q.; Liang, Z. Metallic Bi Nanocrystal-Modified Defective BiVO4 Photoanodes with Exposed (040) Facets for Photoelectrochemical Water Splitting. *ChemElectroChem* **2017**, *4*, 2852−2861.
(43) He, W.; Wang, R.; Zhang, L.; Zhu, J.; Xiang, X.; Li, F. Enhanced Photoelectrochemical Water Oxidation on a BiVO 4 Photoanode Modified with Multi-Functional Layered Double Hydroxide Nanowalls. *J. Mater. Chem. A* **2015**, *3*, 17977−17982.
(44) Qin, M.; Ren, W.; Jiang, R.; Li, Q.; Yao, X.; Wang, S.; You, Y.; Mai, L. Highly Crystallized Prussian Blue with Enhanced Kinetics for Highly Efficient Sodium Storage. *ACS Appl. Mater. Interfaces* **2021**, *13*, 3999−4007.
(45) Samain, L.; Gilbert, B.; Grandjean, F.; Long, G. J.; Strivay, D. Redox Reactions in Prussian Blue Containing Paint Layers as a Result of Light Exposure. *J. Anal. At. Spectrom.* **2013**, *28*, 524−535.
(46) Gabrielli, C. Once upon a Time There Was EIS. *Electrochim. Acta* **2020**, *331*, No. 135324.
(47) Liu, Y.; Guo, Y.; Schelhas, L. T.; Li, M.; Ager, J. W. Undoped and Ni-Doped CoOx Surface Modification of Porous BiVO4 Photoelectrodes for Water Oxidation. *J. Phys. Chem. C* **2016**, *120*, 23449−23457.
(48) Liu, J.; Chen, W.; Sun, Q.; Zhang, Y.; Li, X.; Wang, J.; Wang, C.; Yu, Y.; Wang, L.; Yu, X. Oxygen Vacancies Enhanced WO $_3$ /BiVO $_4$ Photoanodes Modified by Cobalt Phosphate for Efficient Photoelectrochemical Water Splitting. *ACS Appl. Energy Mater.* **2021**, *4*, 2864−2872.
(49) Tang, F.; Cheng, W.; Su, H.; Zhao, X.; Liu, Q. Smoothing Surface Trapping States in 3D Coral-Like CoOOH-Wrapped-BiVO4 for Efficient Photoelectrochemical Water Oxidation. *ACS Appl. Mater. Interfaces* **2018**, *10*, 6228−6234.
(50) Kahraman, A.; Vishlaghi, M. B.; Baylam, I.; Ogasawara, H.; Sennaroğlu, A.; Kaya, S. The Fast-Track Water Oxidation Channel on BiVO $_4$ Opened by Nitrogen Treatment. *J. Phys. Chem. Lett.* **2020**, *11*, 8758−8764.
(51) McNeill, C. R.; Hwang, I.; Greenham, N. C. Photocurrent Transients in All-Polymer Solar Cells: Trapping and Detrapping Effects. *J. Appl. Phys.* **2009**, *106*, No. 024507.
(52) Sivula, K. Mott−Schottky Analysis of Photoelectrodes: Sanity Checks Are Needed. *ACS Energy Lett.* **2021**, *6*, 2549−2551.
(53) Liu, G.; Shi, J.; Zhang, F.; Chen, Z.; Han, J.; Ding, C.; Chen, S.; Wang, Z.; Han, H.; Li, C. A Tantalum Nitride Photoanode Modified with a Hole-Storage Layer for Highly Stable Solar Water Splitting. *Angew. Chem., Int. Ed.* **2014**, *53*, 7295−7299.